

Comparative study on the performance of two synthetic zeolite 4A on the removal of heavy metals from aqueous solution—effect of coal fly ash as Al and Si source

Luiz Thiago Vasconcelos da Silva^a, Armando Diego Lima de Freitas^b, Thaizy de Gois Martins^b, Antônia Mayza de Moraes França^a, Adonay Rodrigues Loiola^b, Ronaldo Ferreira do Nascimento^{a,*}

^aDepartment of Analytical Chemistry and Physical Chemistry, Federal University of Ceará, Fortaleza CEP 60.440-900, CE, Brazil, emails: ronaldo@ufc.br (R.F. do Nascimento), thiago97@alu.ufc.br (L.T.V. da Silva), mayzauece@gmail.com (A.M. de Moraes França)

^bDepartment of Organic and Inorganic Chemistry, Federal University of Ceará, Fortaleza CEP 60.440-900, CE, Brazil, emails: adiego13.dl@gmail.com (A.D.L. de Freitas), thaizygois@gmail.com (T. de Gois Martins), adonay@ufc.br (A.R. Loiola)

Received 16 May 2023; Accepted 31 August 2023

ABSTRACT

Pollution of water bodies from improper disposal of toxic metal contaminated effluents causes several problems for the environment. Several processes can be used to remove these metal ions from aqueous media, and the adsorption being the most efficient technique. In this process, a diversity of adsorbent materials is used, with the use of zeolite 4A emphasized in this study. This study aimed to evaluate the efficiency of zeolite 4A as an adsorbent material for the removal of Cu^{2+} , Cd^{2+} , Pb^{2+} , and Zn^{2+} from aqueous media. For this, zeolite 4A was synthesized by the hydrothermal route starting from two sources of precursors, one from standard reagents (ZA-P) and the other from coal fly ash (ZA), a residue from a thermoelectric industry plant in the state of Ceará (Brazil). Both materials were characterized by X-ray diffraction, scanning electron microscopy, Fourier-transform infrared spectroscopy, and cation exchange capacity techniques. The materials were subjected to batch adsorption tests with multi-element synthetic solutions of Pb^{2+} , Cu^{2+} , Zn^{2+} , and Cd^{2+} . The parameters investigated in the adsorption experiments were the dosage effect, contact time, and adsorption equilibrium. Flame atomic absorption spectroscopy was used for metal ion quantitation. The characterization results showed that both ZA-P and ZA yielded mainly the crystalline phase of zeolite 4A. In the dosage test, a weight of 100 mg promoted the best results for both ZA-P and ZA, with ZA achieving superior removal results. Pb^{2+} was more efficiently removed at 95% for ZA and 93% for ZA-P. In addition, at the time of contact, it was observed that ZA reached equilibrium faster (10 min) than ZA-P (50 min). In the adsorption equilibrium, the Langmuir model was able to describe almost all results, only the Zn^{2+} for ZA was modeled by the Freundlich isotherm. The affinity of metal ions for materials followed the order ($\text{Pb}^{2+} > \text{Cd}^{2+} > \text{Zn}^{2+} > \text{Cu}^{2+}$) for ZA-P and ($\text{Pb}^{2+} > \text{Cd}^{2+} > \text{Cu}^{2+} > \text{Zn}^{2+}$) for ZA. Finally, it is concluded that both products have potential for application as metal adsorbents of Cu^{2+} , Cd^{2+} , Pb^{2+} , and Zn^{2+} in aqueous solutions and that coal fly ash can be recycled to obtain zeolite.

Keywords: Adsorption of metals; Coal fly ash; Zeolite synthetic; Hydrothermal synthesis

* Corresponding author.

1. Introduction

Several toxic metals are constantly released into the environment as industrial waste, causing serious soil and water pollution [1]. Industrialization in developing countries has caused environmental degradation due to the release of heavy metals and other pollutants into the ecosystem [2]. Industries such as battery building, electroplating, paper, textiles, civil construction, etc., discharge effluents containing toxic metals in aquatic ecosystems [3]. These toxic metals are non-biodegradable, toxic, and cause many problems for human health. Major contaminants are chromium (Cr^{6+}), lead (Pb^{2+}), mercury (Hg^{2+}), nickel (Ni^{3+}), copper (Cu^{2+}), zinc (Zn^{2+}), and cadmium (Cd^{2+}) [1,3,4]. Ingestion of toxic metals generates serious problems for human health, such as vomiting, nausea, anaemia, disorders of the central nervous system, stomach cramps, skin irritations, convulsions, cancer, etc. [4,5]. Therefore, there is a strong need to remove these toxic metals from industrial effluents for the protection of the ecosystem, human, and aquatic life. There are numerous processes that have been developed for the removal of dissolved toxic metals, including ion exchange, precipitation, phytoextraction, ultrafiltration, reverse osmosis, electrodialysis, separation membranes, and adsorption [6–11]. The adsorption process is economical, simple in practical operation, ecologically friendly and of high efficacy compared with other methods, such as chemical precipitation, ultrafiltration, membrane filtration, and coagulation [5,12,13]. The use of low-cost alternative materials as adsorbents for the removal of toxic metals is widely researched. Zeolite as one of these is an attractive adsorbent material because of its unique characteristics: ion exchange capacity, affinity for toxic metals, and proven chemical and mechanical stability [14–16].

Zeolites are microporous structures of aluminium silicates with three-dimensional corner-sharing network tetrahedrons $[\text{TO}_4]$, where T usually represents silicon or aluminium [15]. The structure composed of purely $[\text{SiO}_4]$ units is neutral, however, when Al is an isomorph substitute for Si, the structure becomes negatively charged, compensated by extra structural cations (sodium, potassium, or calcium), leading to its cation exchange capacity. Currently, more than 220 different types of zeolite structures are known, and the Si/Al ratio can be adjusted, significantly affecting the characteristics of the material, including cation exchange capacity. Type A zeolite with composition and topology LTA $[\text{Na}_{12}(\text{H}_2\text{O})_{27}]_8[\text{Al}_{12}\text{Si}_{12}\text{O}_{48}]_{87}$ has the lowest Si/Al ratio of 1:1 and exhibits exceptionally high cation exchange capacity and adsorbent performance [17,18].

Zeolites can be synthesized by different methods, among which hydrothermal synthesis stands out and consists of the addition of precursors based on Si and Al to a mineralizing agent, usually hydroxides of alkaline metals. After mixing the precursors with the mineralizing agent solution, a synthesis gel is formed that, when heated and under the appropriate conditions, promotes the crystallization of zeolite in the desired structure [15,18,19].

Coal fly ash is formed by the combustion of coal in thermoelectric plants as a residual product [20–23]. The current annual production of coal fly ash worldwide is estimated at about 780 million tons [23,24]. Efficient elimination of

charcoal fly ash is a global issue due to its massive volume and harmful effects on the environment [22,23,25].

The conversion of fly ash into zeolites is one of the possible alternatives for the recycling of this waste because it contains high levels of silica and alumina which are the fundamental basis of zeolites [26–30].

Therefore, the efficiency of the application of standard zeolite, and zeolite synthesized from coal fly ash in the removal of Pb^{2+} , Cu^{2+} , Zn^{2+} , and Cd^{2+} from an aqueous medium was evaluated and compared in this work. Studies were conducted to verify the influence of dosage and contact time on the materials. In addition, an equilibrium study was conducted to evaluate the mechanism of the process of adsorption.

2. Materials and methods

2.1. Reagents

The inorganic reagents were provided by dynamics as analytical grade reagents. The metal ions studied were Pb(II), Cu(II), Zn(II), and Cd(II). The synthetic solutions of copper, cadmium, lead, and zinc were prepared using their respective nitrate salts, $\text{Cu}(\text{NO}_3)_2 \cdot 3\text{H}_2\text{O}$, $\text{Cd}(\text{NO}_3)_2 \cdot 4\text{H}_2\text{O}$, $\text{Pb}(\text{NO}_3)_2$, and $\text{Zn}(\text{NO}_3)_2 \cdot 6\text{H}_2\text{O}$ in acetate buffer ($\text{CH}_3\text{COOH}/\text{CH}_3\text{COONa}$) solution (pH = 5.0).

2.2. Zeolite 4A synthesis

A hydrothermal synthetic route with two different aluminium and silicon sources was used to obtain zeolite 4A. One material was synthesized from standard reagents, named ZA-P and the other material from coal fly ash, named ZA. The molar composition of the zeolite 4A reaction mixture is known ($3,165 \text{ Na}_2\text{O} : \text{Al}_2\text{O}_3 : 1,926 \text{ SiO}_2 : 128 \text{ H}_2\text{O}$) [31].

In the first case, zeolite ZA-P was synthesized based on the methodology described in verified syntheses of zeolitic materials [32]. Initially, 13.5 g of sodium metasilicate (Na_2SiO_3) and 7.22 g of sodium aluminate (NaAlO_2) were solubilized separately in 35 mL of sodium hydroxide solution ($4.35 \text{ mol} \cdot \text{L}^{-1}$ for each salt). The Na_2SiO_3 solution was added to the NaAlO_2 solution, leading to the formation of a white colored mixture. This mixture was placed in a stainless-steel autoclave with an internal Teflon coating and heated in an oven at 95°C for 4 h, with the objective of obtaining crystallized zeolite 4A. The system was cooled and the material resulting from the synthesis was washed successively with deionized water through the centrifugation process until completely neutralized. Finally, the material was placed in the oven at 80°C for 12 h for drying.

ZA was synthesized as described in previous work which used coal fly ash as an alternative to aluminium and silicon [27,30,33]. The coal fly ash used was supplied by the thermal power plants of the ENEVA group (Pécem, Ceará, Brazil). The fly ash underwent a magnetization process as a pre-treatment and was subsequently separated into portions to remove metals and salts that could interfere in the silica and alumina extraction processes [34]. The NMF portion resulting from the magnetization process was used in the synthesis. Initially, 10 g of ash NMF underwent an extraction process to solubilize the required components,

Si and Al, with 65.5 mL of sodium hydroxide (4.35 mol·L⁻¹), which were stirred for 1 h in a glycerine bath (90°C). After this procedure, the resulting solution was centrifuged to separate the supernatant from the precipitate. To the supernatant, 1.34 g of sodium aluminate (NaAlO₂) were added to adjust the molar composition of the reaction mixture [31]. Moreover, NaOH (4.35 mol·L⁻¹) was added to adjust the volume to 65.5 mL. Following this, the hydrothermal route applied to ZA-P was used again to obtain ZA.

2.3. Material characterization

The synthesized materials, ZA-P and ZA were characterized by X-ray diffraction (XRD), scanning electron microscopy (SEM), X-ray dispersive energy (EDX), cation exchange capacity (CTC), and infrared spectroscopy with Fourier transform (FTIR).

2.4. Batch adsorption study

2.4.1. Dosage study

This study aimed to verify the effect of the concentration of adsorbent material on the removal of Cu²⁺, Cd²⁺, Pb²⁺, and Zn²⁺, and thus find the optimal dosage of material for the removal of the metal ions. In this sense, the effect of the dosage was verified by putting in contact 25 mL of a multi-metallic solution (100 mg·L⁻¹) with different masses of the adsorbent materials (0.01, 0.03, 0.05, 0.07, 0.09, and 0.10 g) in duplicate, obtaining the following dosages 0.04, 1.2, 2.0, 2.8, 3.6, and 4.0 g·L⁻¹, respectively. The system was kept under agitation at 200 rpm for 120 min. The material was filtered, and the residual solutions were analyzed to determine the percent removal of metal ions using flame atomic absorption spectrometry (FAAS). The adsorption capacity (Q_e), which is the amount of ions adsorbed by the adsorbent mass and the removal percent (%R) were evaluated using Eqs. (1) and (2), respectively.

$$Q_e = \frac{C_0 - C_e}{m} \times V \quad (1)$$

$$\%R = \frac{C_0 - C_e}{C_0} \times 100 \quad (2)$$

where Q_e is the adsorption capacity (mg·g⁻¹), m is the used mass of adsorbent (g), V is the solution volume (L) and C₀ and C_e are the metal ion concentrations in the initial solution and in the equilibrium (mg·L⁻¹), respectively, and %R is the removal percentage.

2.4.2. Contact time study

The contact time of the adsorbent materials with the multi-metallic solution, its effect on the removal of metal ions, and the contact time to achieve the best removal from metal ions were studied using a fixed mass of 0.1 g of ZA-P and ZA in batch, in duplicate. The material was placed in contact with 25 mL of a multi-metallic solution (100 mg·L⁻¹) with stirring at 200 rpm for predetermined intervals (0.5, 1, 3, 5, 7, 10, 20, 30, 50, and 60 min.). The final solutions were filtered and analyzed by FAAS, and using Eq. (2), the percent of removal of metal ions by adsorbent materials was calculated.

2.4.3. Adsorption isotherm

The adsorption equilibrium isotherms were obtained using multi-metallic solutions of different concentrations (10, 25, 30, 50, 100, 200, and 500 mg·L⁻¹) in batch (duplicate). The studies were conducted using 25 mL of the metal ion solutions and 0.1 g of the adsorbent materials and were kept under agitation at 200 rpm for 60 min, at room temperature (28°C ± 2°C). Thereupon, the aliquots were filtered, and the residual concentration was analyzed by FAAS.

The results obtained experimentally were evaluated using the non-linearized equations of Langmuir and Freundlich [35,36].

Eq. (3) represents the nonlinear form of the theoretical model of the Langmuir isotherm, where, Q_e (mg·g⁻¹) is the amount adsorbed per gram of adsorbent, K_L (L·mg⁻¹) is the equilibrium constant corresponding to free adsorption energy in the interaction between the surface of the adsorbent and adsorbate, Q_{max} (mg·g⁻¹) is the maximum adsorption capacity and C_e (mg·L⁻¹) is the concentration of adsorbate at equilibrium [35].

$$Q_e = \frac{K_L C_0 Q_{\max}}{1 + C_e K_L} \quad (3)$$

The parameters K_L and Q_{max} depend on the adsorbent material and can be used to compare the performance of adsorbent materials [37].

The nonlinear form of the Freundlich isotherm theoretical model is represented by Eq. (4), where Q_e (mg·g⁻¹) is the amount of adsorbed solute, K_f ((mg·g⁻¹)(L·mg⁻¹)^{1/n}) is the adsorbate adsorption capacity constant, C_e (mg·L⁻¹) is the equilibrium concentration in solution and 1/n is a constant related to the heterogeneity of the surface [36].

$$Q_e = K_f C_e^{1/n} \quad (4)$$

Favorable adsorption tends to have a value of n between 1 and 10. The higher the value of n (the lower value of 1/n), the stronger the interaction between the adsorbate and the adsorbent [38].

2.4.4. Determination of metal ions

The determination of the concentration of metal ions was performed using flame atomic absorption spectrometry (FAAS), with VARIAN 24ZOFs spectrophotometer equipment. The gas mixture used was Ar-Acetylene and the resonance wavelengths were for Cu²⁺ (324.7 nm), Cd²⁺ (228.8 nm), Pb²⁺ (217.0 nm), and Zn²⁺ (213.9 nm), with the linear concentration range for each metal ion used for the calibration curve being from 0.03 to 10 mg·L⁻¹.

3. Results

3.1. Synthesis and characterization

3.1.1. X-ray diffraction

According to the diffractograms of ZA-P and ZA (Fig. 1), it was observed that the peaks agreed with the diffraction peaks of the 4A zeolite pattern most intense at angles 2θ

of 7.24° and 35.30° [39]. In addition, it was found that the synthesized zeolites were identified as a single crystalline phase, free of impurities, as shown by the identification of the peaks using the ICSD 088329 database.

3.1.2. Scanning electron microscopy

The micrographs (Fig. 2) showed that the zeolites are composed of clusters of small particles with a uniform size in the order of $1\ \mu\text{m}$, presenting the symmetry of cubic crystals as well as morphology as well-defined edges characteristic of the phase of zeolite 4A [15,40,41].

3.1.3. X-ray dispersive energy and cation exchange capacity

According to the percentage of Si and Al for each synthesized zeolite obtained through the semi-quantitative analysis of X-ray dispersive energy (EDX) (Table 1), it was possible to establish a Si/Al ratio of 1.069 and 0.947 for ZA-P and ZA, respectively, indicating similarity with the Si/Al ratio of zeolite 4A obtained in other studies [42,43].

In general, the Si/Al ratio has a great influence on the CTC of zeolites. In this sense, it is reported in the literature that the low Si/Al ratio intensifies the cation exchange process due to the higher percentage of Al, which favors the structure having relatively high amounts of negative charges [44]. Thus, it is suggested that the ZA should have a greater CTC when compared with the ZA-P since it has a higher Si/Al ratio, which has been proven with the results of CTC.

To determine the material CTC, a methodology described elsewhere was applied [45]. In this sense, it was observed

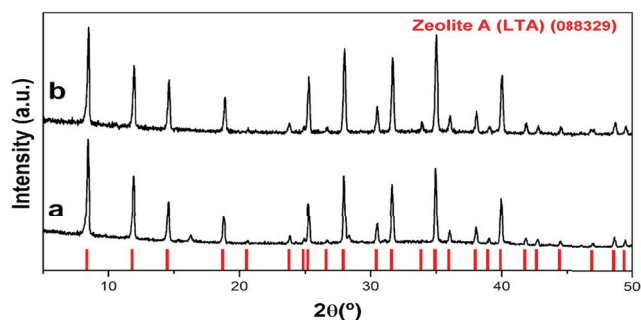


Fig. 1. X-ray diffractogram for (a) ZA-P and (b) ZA.

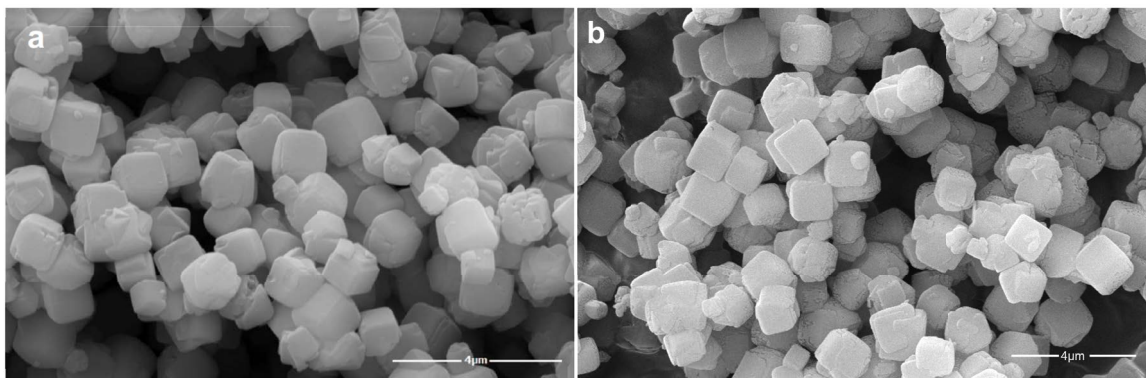


Fig. 2. Scanning electron micrograph for (a) ZA-P and (b) ZA.

that part of the Na^+ present in 1.0 g of the materials was replaced by NH_4^+ . Therefore, this incorporation of 23 and 39 mg for ZA-P and ZA of NH_4^+ , respectively, is equivalent to $127\ \text{meq}\cdot 100\cdot\text{g}^{-1}$ ZA-P and $214\ \text{meq}\cdot 100\cdot\text{g}^{-1}$ ZA. The CTC results for ZA-P and ZA corresponded, respectively, to 23% and 39% of the theoretical value ($547\ \text{meq}\cdot 100\cdot\text{g}^{-1}$), based on the molecular formula of zeolite 4A. These low CTC values for the zeolites under study may be related to the water adsorbed on the material, which is generally much higher than that presented in the literature, suggesting that the CTC is higher than that found experimentally [46].

3.1.4. Infrared spectroscopy with Fourier transform

According to the FTIR spectra (Fig. 3), the absorption bands $3,440$ and $1,649\ \text{cm}^{-1}$ refer to the symmetrical stretching

Table 1
Elementary percentage for Si and Al in ZA-P and ZA acquired from EDX

Samples	%Si	%Al	Si/Al	CEC ($\text{meq}\cdot 100\cdot\text{g}^{-1}$)
ZA-P	19.90	17.90	1.069	127
ZA	18.66	18.89	0.947	214

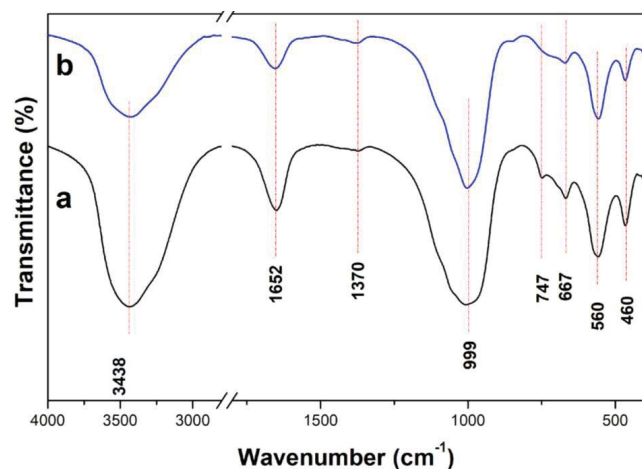


Fig. 3. Infrared spectrum in KBr of (a) ZA-P and (b) ZA.

$\nu_{(\text{O-H})}$ and angular deformation $\delta_{(\text{O-H})}$ of the $-\text{OH}$ bond of the water molecule adhered to the surface of the materials due to medium humidity [47,48]. The band present around $1,000\text{ cm}^{-1}$ is related to internal vibrations of the asymmetric stretching of the T–O connections, $\nu_a(\text{T-O})$, $\nu_s(\text{T} = \text{Si}$ or $\text{Al})$, whereas the bands present in the regions between 400 and 700 cm^{-1} are associated with typical vibrations of the secondary construction units of nanostructured material, known as the fingerprint of each zeolite. Therefore, the bands 461 , 560 , and 664 cm^{-1} are related to the deformation vibration of the external T–O connections $\delta(\text{T-O})$, deformation vibrations in the D4-R rings, $\nu\text{D4-R}$, and symmetrical T–O stretching vibrations of the internal zeolite tetrahedrons, $\nu_s(\text{T-O})$ [49,50]. The results indicated similarity with previous studies [15,30,51] (Table 2).

3.2. Batch adsorption study

3.2.1. Dosage study

The amount of adsorbent is an important factor that determines the adsorption capacity for a given concentration of adsorbates [52–55].

For both materials the adsorption capacity was inversely proportional to the material dosage, that is, the increase in dosage caused a decrease in the adsorption capacity

(Fig. 4), this behavior occurs because the increase in adsorbent dosage increases the availability of active sites in the adsorbent, providing greater removal of metal ions from the solution [56,57]. In addition, when the adsorbent is in high dosages, the adsorbents agglomerate and thus decrease the surface area, caused by the overlap of the active sites, making it difficult for the ions to access them, which generates a decrease in the adsorption capacity [58].

The removal of all metal ions was more favorable for ZA than for ZA-P, which was already expected from the

Table 2
Comparison between the absorption bands in the infrared for the studied materials

Assignments	ZA-P (cm^{-1})	ZA (cm^{-1})	[15] (cm^{-1})	[30] (cm^{-1})	[51] (cm^{-1})
$\nu_{(\text{O-H})}$ water	3,440	3,440	3,420	3,420	3,436
$\delta_{(\text{O-H})}$ water	1,649	1,649	1,623	1,621	1,653
$\nu_a(\text{T-O})$	1,005	1,005	1,000	999	1,002
$\nu_s(\text{T-O})$	664	664	674	662	662
$\nu\text{D4-R}$	560	560	555	552	552
$\delta(\text{T-O})$	460	460	468	461	461

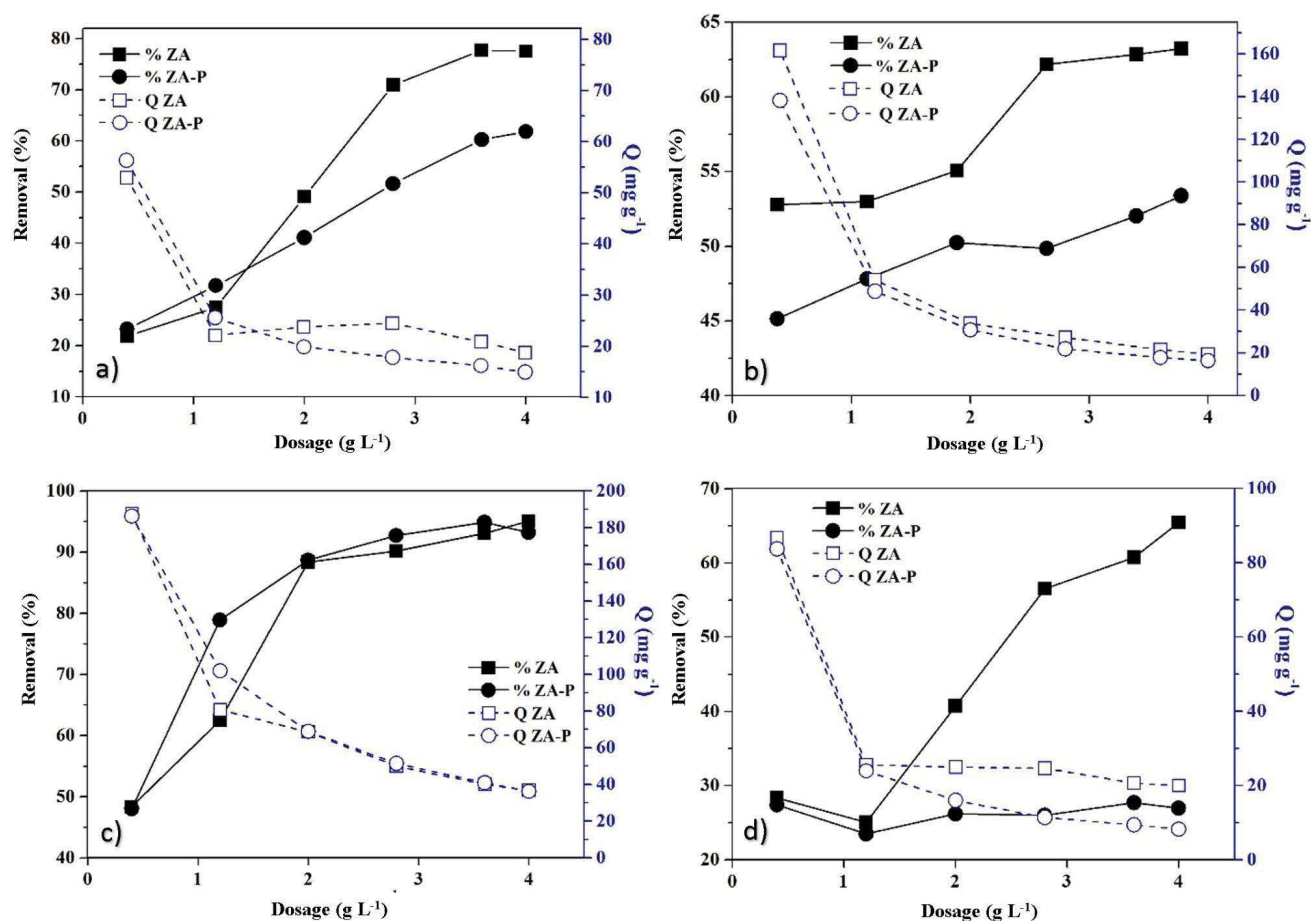


Fig. 4. Effect of ZA and ZA-P zeolite dosage on adsorption capacity and metal ion removal: (a) Cd^{2+} , (b) Cu^{2+} , (c) Pb^{2+} , and (d) Zn^{2+} (temperature $28^\circ\text{C} \pm 2^\circ\text{C}$; stirring speed, 200 rpm; volume, 25 mL; concentrations of metal ions, $100\text{ mg}\cdot\text{L}^{-1}$; time, 120 min).

characterization of the materials, whose CTC and EDX showed that ZA had a more electronegative structure than ZA-P.

It can be observed in Fig. 4c, that Pb^{2+} is the metal ion with the highest removal for both materials, obtaining values close to 95% for ZA and 93% for ZA-P for the highest dosage ($4 \text{ g}\cdot\text{L}^{-1}$). The metal ion with the intermediate selective behavior was Cd^{2+} (Fig. 4a), with removal of approximately 77% and 62% for ZA and ZA-P, respectively. However, Cu^{2+} (Fig. 4b), and Zn^{2+} (Fig. 4d), were the metal ions with the least selective behavior for ZA and ZA-P, respectively, with removal values close to 63% and 27%, respectively. In addition, Zn^{2+} , presented the greatest removal difference between the materials (Fig. 4d) about 38.5%. Therefore, the highest dosage of $4 \text{ g}\cdot\text{L}^{-1}$ (0.1 g) was chosen as the optimal dosage for the other adsorption tests for both materials as it obtained the best removal results.

3.2.2. Contact time study

Contact time can describe the adsorption kinetics, i.e. it reflects the influence of time on the adsorption process of a certain concentration of adsorbate and on the achievement of the adsorption equilibrium [52,54,59].

The adsorption in the 5 min occurs quickly, reaching removal values of 85% of Cd^{2+} in the ZA and 65% of Pb^{2+} in the ZA-P, however the level of adsorption equilibrium for both materials is not yet observed in this time interval, Fig. 5a and b.

The process of adsorption of metal ions by ZA (Fig. 5a), has a fast adsorption behavior in the 5 min, reaching equilibrium for most metals close to 10 min. The Cd^{2+} reached 90.1% removal with just 7 min of contact, maintaining this high removal range until the end of the 60 min. The Zn^{2+} in 10 min reached removal of about 77%, reaching values close to 81% in 30 min. The adsorbent showed a similar preference for Pb^{2+} and Cu^{2+} , in the first 10 min they reached removal values of 61% and 59.4% and at the end of the 60 min they reached removal values of 57% and 54%, respectively.

The adsorption behavior of ZA-P (Fig. 5b), although fast in the first 10 min, reaches equilibrium for most metals

close to 50 min. The sets of $\text{Pb}^{2+}/\text{Cd}^{2+}$ and $\text{Zn}^{2+}/\text{Cu}^{2+}$ had similar behaviors, in which initially one of the metals had the preference of the adsorbent and over time this preference was changed to the other metal ions.

For the $\text{Pb}^{2+}/\text{Cd}^{2+}$ set, Pb^{2+} reached close to 80% with just 1 min of contact, on the other hand Cd^{2+} in that same time reached close to 35%, however as the contact time increases, the removal of Pb^{2+} decreases and the removal of Cd^{2+} increases, the preference of the adsorbent changes around 20 min and at the end of the 60 min the removal values of Cd^{2+} and Pb^{2+} are 72% and 61%, respectively.

This behavior, according to the literature, is because Cd^{2+} has an ionic hydration radius (4.26 \AA) greater than Pb^{2+} (2.61 \AA), which causes a slower initial adsorption, since in the adsorption the metal with the greatest hydration radius will have to spend more energy to release the water molecules, however the kinetics over time probably change due to the affinity of the metal with the adsorbent surface [60,61]. Therefore, the same explanation can be used to explain the adsorption behavior of the $\text{Zn}^{2+}/\text{Cu}^{2+}$ set, since in the first 5 min Cu^{2+} , which has a smaller hydration radius (2.95 \AA), reached 33% removal, while Zn^{2+} , with a greater hydration radius (4.30 \AA) reached 30%, with 20 min of contact the preference of material changed and at the end of 60 min, Zn^{2+} and Cu^{2+} reached values of 39% and 35%, respectively.

Therefore, the optimum contact time for all metals in both materials was 60 min, as it is the time when all metals were in equilibrium. In addition, the preference of materials for metals was practically similar, alternating only in affinity for metals Pb^{2+} and Zn^{2+} and can be ordered in descending order as $\text{Cd}^{2+} > \text{Zn}^{2+} > \text{Pb}^{2+} > \text{Cu}^{2+}$ and $\text{Cd}^{2+} > \text{Pb}^{2+} > \text{Zn}^{2+} > \text{Cu}^{2+}$ for ZA and ZA-P, respectively.

3.2.3. Adsorption isotherm

The behavior for both materials was similar, in that the increase in the initial concentration of the multielement ions solution, caused an increase in the adsorption capacity of all metal ions by the adsorbents. This behavior is observed because of the phenomenon of the driving force of the system, since in low concentrations, the adsorption

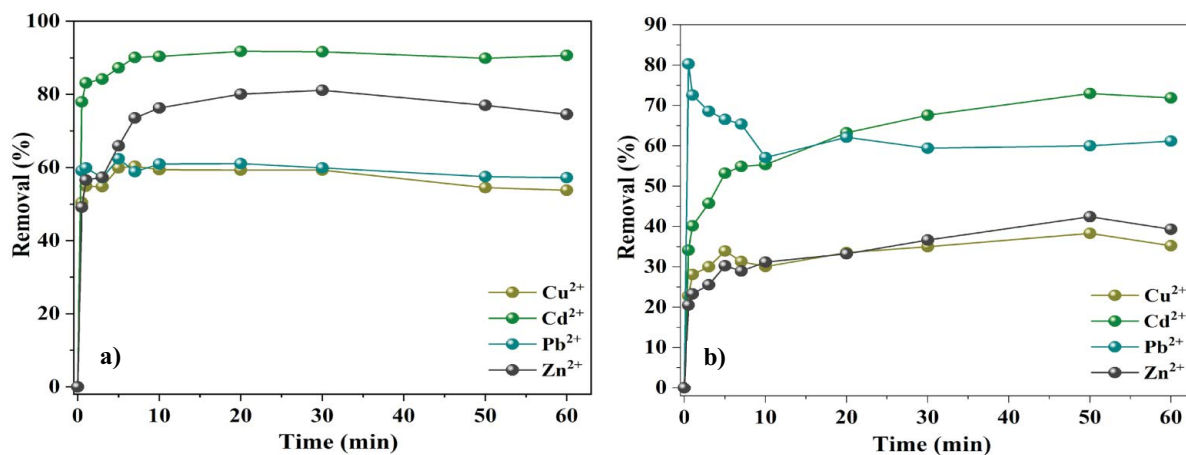


Fig. 5. Effect of contact time on metal ion removal (a) ZA (b) ZA-P (temperature, $28^\circ\text{C} \pm 2^\circ\text{C}$; stirring speed, 200 rpm; volume, 25 mL; concentrations of metal ions, $100 \text{ mg}\cdot\text{L}^{-1}$; dosage, $4 \text{ g}\cdot\text{L}^{-1}$).

sites are more available, leading to an increase in the concentration gradient and in the solute diffusion speed to the adsorbent [62].

The main parameter used in this study to verify the suitability of the isotherm models for each metal ion

adsorption profile, for the different materials, was the determination coefficient (R^2), based expressly on the values of the SSE error function.

According to Fig. 6 and Table 3, it is noted that all metal ions studied for the adsorption of ZA-P, are

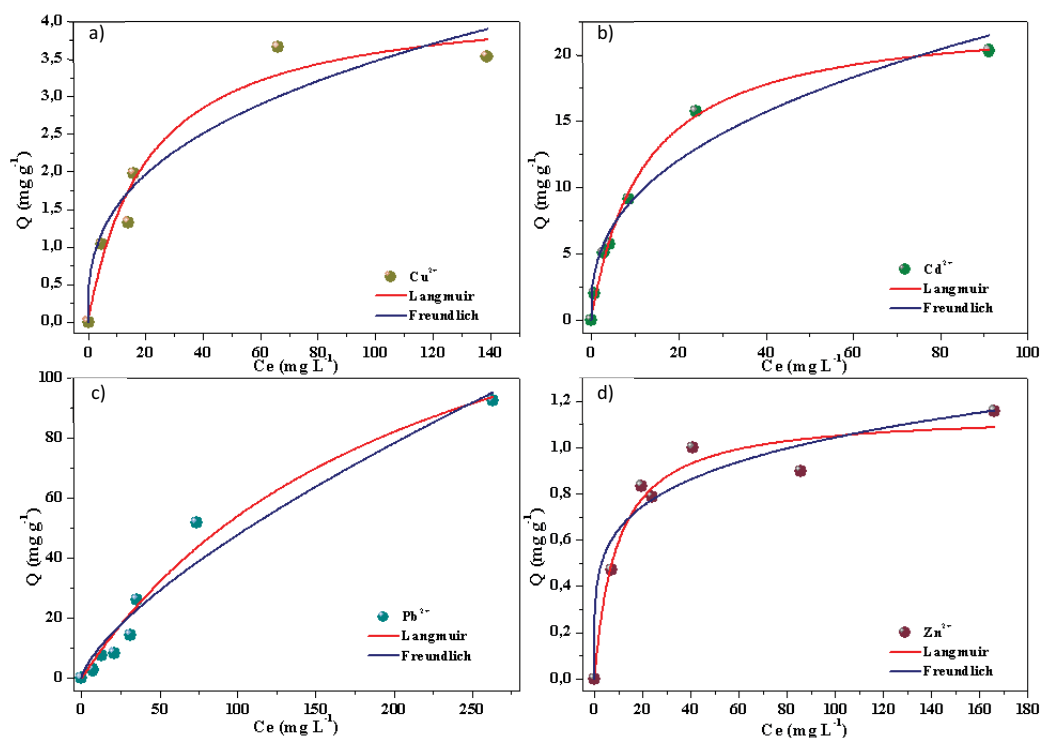


Fig. 6. Multielement adsorption isotherm for ZA-P of metal ions (a) Cu^{2+} , (b) Cd^{2+} , (c) Pb^{2+} and (d) Zn^{2+} (pH = 5.0; temperature, $28^\circ\text{C} \pm 2^\circ\text{C}$; stirring speed, 200 rpm; volume, 25 mL; dosage, $4 \text{ g}\cdot\text{L}^{-1}$).

Table 3

Parameters of the ion adsorption isotherm models (Pb^{2+} , Cd^{2+} , Zn^{2+} , and Cu^{2+}) in the ZA-P and ZA, multielement system

Material	Isotherms models	Parameters	Pb^{2+}	Cd^{2+}	Zn^{2+}	Cu^{2+}
ZA-P	Langmuir	Q_{exp} ($\text{mg}\cdot\text{g}^{-1}$)	92.35	20.28	1.16	3.65
		$Q_{\text{m\acute{a}x}}$ ($\text{mg}\cdot\text{g}^{-1}$)	170 ± 29.7	23 ± 0.75	1.15 ± 0.075	4.305 ± 0.45
		K_L	0.0047 ± 0.0014	0.0841 ± 0.008	0.10712 ± 0.031	0.048 ± 0.015
		R^2	0.9703	0.9945	0.9548	0.9465
		SSE	29.89	0.2995	0.0068	0.1113
	Freundlich	n	1.407 ± 12.25	2.63 ± 21.74	4.813 ± 19.84	2.831 ± 12.94
		K_f	1.815 ± 0.78	3.86 ± 0.68	0.40 ± 0.083	0.6815 ± 0.22
		R^2	0.9472	0.9536	0.9244	0.9076
		SSE	53.23	2.510	0.0113	0.1924
		ZA	Langmuir	Q_{exp} ($\text{mg}\cdot\text{g}^{-1}$)	105.51	13.687
$Q_{\text{m\acute{a}x}}$ ($\text{mg}\cdot\text{g}^{-1}$)	164.82 ± 9.76			13.27 ± 0.654	10.76 ± 1.50	4.683 ± 0.204
K_L	0.0080 ± 0.00095			0.6851 ± 0.158	0.1139 ± 0.05	0.558 ± 0.145
R^2	0.9943			0.9685	0.8518	0.9668
SSE	7.2491			0.8494	2.2343	0.0998
Freundlich	n		1.59 ± 20.7	5.16 ± 37.3	4.46 ± 20.45	7.004 ± 28.7
	K_f		3.55 ± 0.048	5.87 ± 0.59	2.904 ± 0.695	2.53 ± 0.32
	R^2		0.9772	0.9521	0.8710	0.9227
	SSE		28.87	1.2911	1.9446	0.2326

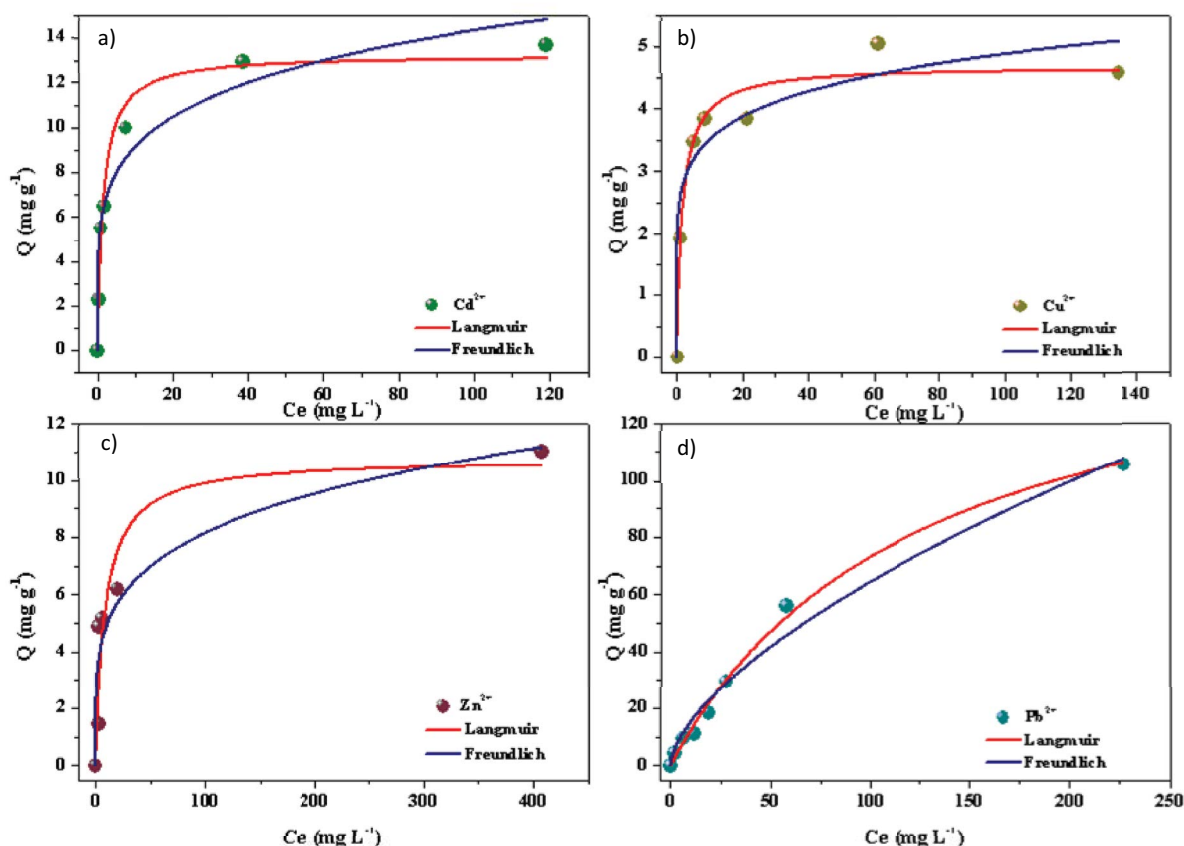


Fig. 7. Multielement adsorption isotherm for ZA of metal ions (a) Cd^{2+} , (b) Cu^{2+} , (c) Zn^{2+} and (d) Pb^{2+} (pH = 5.0; temperature, $28^\circ\text{C} \pm 2^\circ\text{C}$; stirring speed, 200 rpm; volume, 25 mL; dosage, $4 \text{ g}\cdot\text{L}^{-1}$).

better described by the Langmuir model. In the case of ZA (Fig. 7 and Table 3), the isothermal adsorption models were adjusted differently for metal ions. The adsorption profiles of Pb^{2+} , Cu^{2+} , and Cd^{2+} were adjustable to the Langmuir model. On the other hand, Zn^{2+} was better suited to the Freundlich model. The suitability of the Langmuir model suggests a homogeneity in the energy of the adsorbent sites and a monolayer adsorption process [63,64]. On the other hand, the suitability of the Freundlich model suggests the presence of several types of adsorption sites, that present different adsorptive energies [65].

Within the model parameters, it can be highlighted those that manage to express the magnitude of affinity in the adsorption process, that is the degree of interaction between the adsorbate and the adsorbent sites, whose in the Langmuir model is the Langmuir constant (K_L) and in the Freundlich model it is the constant n , in which the favorable process has values between 1 and 10 model [38,66]. According to the values of K_L , the order of affinity with ZA-P is $\text{Zn}^{2+} > \text{Cd}^{2+} > \text{Cu}^{2+} > \text{Pb}^{2+}$ and according to n values the order with ZA-P is $\text{Zn}^{2+} > \text{Cu}^{2+} > \text{Cd}^{2+} > \text{Pb}^{2+}$. In the same way, for ZA, according to the constant K_L , the adsorption process followed the order $\text{Cd}^{2+} > \text{Cu}^{2+} > \text{Zn}^{2+} > \text{Pb}^{2+}$ and according to the constant n the affinity had the order $\text{Cu}^{2+} > \text{Cd}^{2+} > \text{Zn}^{2+} > \text{Pb}^{2+}$. Thus, for all the metal ions studied, the process was favorable, that is the concentration of metals in the liquid phase is considerably lower than on the surface of the adsorbent.

Regarding the maximum adsorption capacity for ZA-P in the Langmuir model (Q_{max}) it was observed that the affinity of the material follows the following order $\text{Pb}^{2+} > \text{Cd}^{2+} > \text{Cu}^{2+} > \text{Zn}^{2+}$, while the Freundlich constant K_f , which indicates the capacity of adsorption in this model, presents a different order ($\text{Cd}^{2+} > \text{Pb}^{2+} > \text{Cu}^{2+} > \text{Zn}^{2+}$). The same behavior was observed for ZA, with Q_{max} and K_f in which the orders were $\text{Pb}^{2+} > \text{Cd}^{2+} > \text{Zn}^{2+} > \text{Cu}^{2+}$ and $\text{Cd}^{2+} > \text{Pb}^{2+} > \text{Zn}^{2+} > \text{Cu}^{2+}$. This antagonistic behavior was observed in another study, in which different results were obtained for Q_{max} and K_f respectively for $\text{Cu}^{2+} > \text{Pb}^{2+} > \text{Zn}^{2+} > \text{Cd}^{2+}$ and $\text{Pb}^{2+} > \text{Cu}^{2+} > \text{Cd}^{2+} > \text{Zn}^{2+}$ using magnetic zeolite adsorbent material [30].

4. Conclusions

According to the DRX, SEM/EDX, CTC, and FTIR characterization results zeolitic materials were successfully produced for both Si and Al sources, standard reagents, and coal fly ash. For the dosage test, it was possible to conclude that the optimum dosage for both materials was $0.4 \text{ g}\cdot\text{L}^{-1}$ (0.1 g), with ZA zeolite obtaining the best removal results for all metal ions. The contact time test showed that ZA achieved an equilibrium time of 10 min, being faster than ZA-P at 50 min. In the equilibrium study, the materials showed equal selectivity for Pb^{2+} and Cd^{2+} , as well as different selectivity for Zn^{2+} and Cu^{2+} . Zeolite ZA showed the affinity $\text{Pb}^{2+} > \text{Cd}^{2+} > \text{Cu}^{2+} > \text{Zn}^{2+}$ and ZA-P $\text{Pb}^{2+} > \text{Cd}^{2+} > \text{Zn}^{2+} > \text{Cu}^{2+}$.

The Langmuir model was able to model almost all results, only Zn²⁺ for ZA was modelled using Freundlich's expression. Finally, it was possible to conclude that the studied materials can be applied for the adsorption of Pb²⁺, Cd²⁺, Zn²⁺, Cu²⁺ in aqueous solutions. Also, the fly ash of coal, can be recycled to obtain material with a high application value in environmental remediation.

Acknowledgements

The authors would like to thank Ray-X Laboratory and Professor José Marcos Sasaki for XRD analyses and Analytical central-UFC for the SEM analysis (UFC/CT-INFRA/MCTI-SISNANO/Pró-equipamentos-CAPES).

Disclosure statement

No potential conflict of interest was reported by the author(s).

References

- [1] L. Wang, C. Guo, Q. Qian, D. Lang, R. Wu, S. Abliz, W. Wang, J. Wang, Adsorption behavior of UV aged microplastics on the heavy metals Pb(II) and Cu(II) in aqueous solutions, *Chemosphere*, 313 (2023) 137439, doi: 10.1016/j.chemosphere.2022.137439.
- [2] M. Mokarram, A. Saber, V. Sheykhi, Effects of heavy metal contamination on river water quality due to release of industrial effluents, *J. Cleaner Prod.*, 277 (2020) 123380, doi: 10.1016/j.jclepro.2020.123380.
- [3] R. Upadhyay, P.K. Pandey, Pardeep, Adsorption of Cu(II) and Cr(VI) by zeolite in batch and column mode, *Mater. Today Proc.*, 4 (2017) 10504–10508.
- [4] Y. Li, Q. Zhou, B. Ren, J. Luo, J. Yuan, X. Ding, H. Bian, X. Yao, Trends and Health Risks of Dissolved Heavy Metal Pollution in Global River and Lake Water from 1970 to 2017, P. de Voogt, Ed., *Reviews of Environmental Contamination and Toxicology*, Vol. 251, Springer, Cham, 2019. Available at: https://doi.org/10.1007/398_2019_27
- [5] L. Liu, K. Zhang, Nanopore-based strategy for sequential separation of heavy-metal ions in water, *Environ. Sci. Technol.*, 52 (2018) 5884–5891.
- [6] A. Belgacem, R. Rebiai, H. Hadoun, S. Khemaissia, M. Belmedani, The removal of uranium(VI) from aqueous solutions onto activated carbon developed from grinded used tire, *Environ. Sci. Pollut. Res.*, 21 (2014) 684–694.
- [7] L. Fang, L. Li, Z. Qu, H. Xu, J. Xu, N. Yan, A novel method for the sequential removal and separation of multiple heavy metals from wastewater, *J. Hazard. Mater.*, 342 (2018) 617–624.
- [8] Z. Dahaghin, H.Z. Mousavi, S.M. Sajjadi, A novel magnetic ion imprinted polymer as a selective magnetic solid phase for separation of trace lead(II) ions from agricultural products, optimization using a Box–Behnken design, *Food Chem.*, 237 (2017) 275–281.
- [9] Q. Zhou, B. Liao, L. Lin, W. Qiu, Z. Song, Adsorption of Cu(II) and Cd(II) from aqueous solutions by ferromanganese binary oxide–biochar composites, *Sci. Total Environ.*, 615 (2018) 115–122.
- [10] M. Pirveysian, M. Ghiaci, Synthesis and characterization of sulfur functionalized graphene oxide nanosheets as efficient sorbent for removal of Pb²⁺, Cd²⁺, Ni²⁺ and Zn²⁺ ions from aqueous solution: a combined thermodynamic and kinetic studies, *Appl. Surf. Sci.*, 428 (2018) 98–109.
- [11] A.A. Zunaïdi, L.H. Lim, F. Metali, Comparative assessment of the heavy metal phytoextraction potential of vegetables from agricultural soils: a field experiment, *Heliyon*, 9 (2023) e13547, doi: 10.1016/j.heliyon.2023.e13547.
- [12] J. Ali, H. Wang, J. Ifthikar, A. Khan, T. Wang, K. Zhan, A. Shahzad, Z. Chen, Z. Chen, Efficient, stable, selective adsorption of heavy metals by thio-functionalized layered double hydroxide in diverse types of water, *Chem. Eng. J.*, 332 (2018) 387–397.
- [13] M.I. Shariful, S. Talebian, M. Mehrali, B.C. Ang, M.A. Amal, Corrigendum: adsorption capability of heavy metals by chitosan/poly(ethylene oxide)/activated carbon electrospun nanofibrous membrane, *J. Appl. Polym. Sci.*, 135 (2018) 46083.
- [14] S.E. Lehman, S.C. Larsen, Zeolite and mesoporous silica nanomaterials: greener syntheses, environmental applications and biological toxicity, *Environ. Sci. Nano*, 1 (2014) 200–213.
- [15] R.A. Bessa, L. de Sousa Costa, C.P. Oliveira, F. Bohn, R. Ferreira do Nascimento, J.M. Sasaki, A.R. Loiola, Kaolin-based magnetic zeolites A and P as water softeners, *Microporous Mesoporous Mater.*, 245 (2017) 64–72.
- [16] Y. Li, L. Li, J. Yu, Applications of zeolites in sustainable chemistry, *Chem*, 3 (2017) 928–949.
- [17] Z. Yuna, Review of the natural, modified, synthetic zeolites for heavy metals removal from wastewater, *Environ. Eng. Sci.*, 33 (2016) 443–454.
- [18] M. Hong, L. Yu, Y. Wang, J. Zhang, Z. Chen, L. Dong, Q. Zan, R. Li, Heavy metal adsorption with zeolites: the role of hierarchical pore architecture, *Chem. Eng. J.*, 359 (2019) 363–372.
- [19] Y. Hu, X. Liu, Chemical composition and surface property of kaolins, *Miner. Eng.*, 16 (2003) 1279–1284.
- [20] M. Gao, Q. Ma, Q. Lin, J. Chang, H. Ma, Fabrication and adsorption properties of hybrid fly ash composites, *Appl. Surf. Sci.*, 396 (2017) 400–411.
- [21] K.S. Hui, C.Y.H. Chao, S.C. Kot, Removal of mixed heavy metal ions in wastewater by zeolite 4A and residual products from recycled coal fly ash, *J. Hazard. Mater.*, 127 (2005) 89–101.
- [22] F. Mushtaq, M. Zahid, I.A. Bhatti, S. Nasir, T. Hussain, Possible applications of coal fly ash in wastewater treatment, *J. Environ. Manage.*, 240 (2019) 27–46.
- [23] A.K. Tripathy, B. Behera, V. Aishvarya, A.R. Sheik, B. Dash, C.K. Sarangi, B.C. Tripathy, K. Sanjay, I.N. Bhattacharya, Sodium fluoride assisted acid leaching of coal fly ash for the extraction of alumina, *Miner. Eng.*, 131 (2019) 140–145.
- [24] N. Toniolo, A.R. Boccaccini, Fly ash-based geopolymers containing added silicate waste. A review, *Ceram. Int.*, 43 (2017) 14545–14551.
- [25] X. Huang, H. Zhao, G. Zhang, J. Li, Y. Yang, P. Ji, Potential of removing Cd(II) and Pb(II) from contaminated water using a newly modified fly ash, *Chemosphere*, 242 (2020) 125148, doi: 10.1016/j.chemosphere.2019.125148.
- [26] A. Zacco, L. Borgese, A. Gianoncelli, R.P.W.J. Struis, L.E. Depero, E. Bontempi, Review of fly ash inertisation treatments and recycling, *Environ. Chem. Lett.*, 12 (2014) 153–175.
- [27] Q. Qiu, X. Jiang, G. Lv, Z. Chen, S. Lu, M. Ni, J. Yan, X. Deng, Adsorption of heavy metal ions using zeolite materials of municipal solid waste incineration fly ash modified by microwave-assisted hydrothermal treatment, *Powder Technol.*, 335 (2018) 156–163.
- [28] M. Ahmaruzzaman, A review on the utilization of fly ash, *Prog. Energy Combust. Sci.*, 36 (2010) 327–363.
- [29] A.A. Alqadami, Mu. Naushad, M.A. Abdalla, T. Ahamad, Z.A. Alothman, S.M. Alshehri, A.A. Ghfar, Efficient removal of toxic metal ions from wastewater using a recyclable nanocomposite: a study of adsorption parameters and interaction mechanism, *J. Cleaner Prod.*, 156 (2017) 426–436.
- [30] B.A. Santos, A.M. de Moraes França, L.T. Vasconcelos da Silva, A.G. Santana Gouveia, C.B. Vidal, A.R. Loiola, R.F. Nascimento, Magnetic zeolite from fly ash as a cost-effective adsorbent for Cu²⁺, Pb²⁺, Zn²⁺, Cd²⁺ removal from aqueous media: a comprehensive study, *Int. J. Environ. Anal. Chem.*, (2022) 1–23, doi: 10.1080/03067319.2022.2098020.
- [31] R.W. Thompson, A. Dyer, Nucleation of zeolite NaA crystals in hydrothermal systems, *Zeolites*, 5 (1985) 302–308.
- [32] R.W. Thompson, K.C. Franklin, In: H. Robson, K.P. Lillerud, Eds., *Verified Syntheses of Zeolitic Materials*, Elsevier Science, Amsterdam, 2001, pp. 179–181.

- [33] J.D.C. Izidoro, D.A. Fungaro, F.S. dos Santos, S. Wang, Characteristics of Brazilian coal fly ashes and their synthesized zeolites, *Fuel Process. Technol.*, 97 (2012) 38–44.
- [34] S.V. Vassilev, R. Menendez, D. Alvarez, M. Diaz-Somoano, M.R. Martinez-Tarazona, Phase-mineral and chemical composition of coal fly ashes as a basis for their multicomponent utilization. 1. Characterization of feed coals and fly ashes, *Fuel*, 82 (2003) 1793–1811.
- [35] I. Langmuir, The adsorption of gases on plane surfaces of glass, mica and platinum, *J. Am. Chem. Soc.*, 40 (1914) 1361–1403.
- [36] H.M.F. Freundlich, Over the adsorption in solution, *J. Phys. Chem.*, 57 (1906) 385–471.
- [37] O.M. Adedeji, K. Jahan, Removal of pollutants from aqueous product of co-hydrothermal liquefaction: adsorption and isotherm studies, *Chemosphere*, 321 (2023) 138165, doi: 10.1016/j.chemosphere.2023.138165.
- [38] N. Somsesta, V. Sricharoenchaikul, D. Aht-Ong, Adsorption removal of methylene blue onto activated carbon/cellulose biocomposite films: equilibrium and kinetic studies, *Mater. Chem. Phys.*, 240 (2020) 122221, doi: 10.1016/j.matchemphys.2019.122221.
- [39] X. Hu, J. Bai, C. Li, H. Liang, W. Sun, Silver-based 4A zeolite composite catalyst for styrene epoxidation by one-pot hydrothermal synthesis, *Eur. J. Inorg. Chem.*, 2015 (2015) 3758–3763.
- [40] A.A.B. Maia, R.S. Angélica, R.F. Neves, Use of industrial kaolin waste from the Brazilian Amazon region for synthesis of zeolite A, *Clay Miner.*, 46 (2011) 165–175.
- [41] C.I. Round, S.J. Hill, K. Latham, C.D. Williams, The crystal morphology of zeolite A. The effects of the source of the reagents, *Microporous Mater.*, 11 (1997) 213–225.
- [42] S. Gao, H. Peng, B. Song, J. Zhang, W. Wu, J. Vaughan, P. Zardo, J. Vogrin, S. Tulloch, Z. Zhu, Synthesis of zeolites from low-cost feeds and its sustainable environmental applications, *J. Environ. Chem. Eng.*, 11 (2023) 108995, doi: 10.1016/j.jece.2022.108995.
- [43] N. Bouaziz, M. Ben Manaa, F. Aouaini, A. Ben Lamine, Investigation of hydrogen adsorption on zeolites A, X and Y using statistical physics formalism, *Mater. Chem. Phys.*, 225 (2019) 111–121.
- [44] H. Minamisawa, R. Okunugi, M. Minamisawa, S. Tanaka, K. Saitoh, N. Arai, M. Shibukawa, Preconcentration and determination of cadmium by GFAAS after solid-phase extraction with synthetic zeolite, *Anal. Sci.*, 22 (2006) 709–713.
- [45] C.B. Vidal, G.S.C. Raulino, A.L. Barros, A.C.A. Lima, J.P. Ribeiro, M.J.R. Pires, R.F. Nascimento, BTEX removal from aqueous solutions by HDTMA-modified Y zeolite, *J. Environ. Manage.*, 112 (2012) 178–185.
- [46] A.R. Loiola, L.R.D. da Silva, P. Cubillas, M.W. Anderson, Synthesis and characterization of hierarchical porous materials incorporating a cubic mesoporous phase, *J. Mater. Chem.*, 18 (2008) 4985–4993.
- [47] W.-M. Xie, F.-P. Zhou, X.-L. Bi, D.-D. Chen, J. Li, S.-Y. Sun, J.-Y. Liu, X.-Q. Chen, Accelerated crystallization of magnetic 4A-zeolite synthesized from red mud for application in removal of mixed heavy metal ions, *J. Hazard. Mater.*, 358 (2018) 441–449.
- [48] E. Tombácz, pH-dependent surface charging of metal oxides, *Period. Polytech. Chem. Eng.*, 53 (2009) 77–86.
- [49] A.E. Ameh, O.O. Fatoba, N.M. Musyoka, L.F. Petrik, Influence of aluminium source on the crystal structure and framework coordination of Al and Si in fly ash-based zeolite NaA, *Powder Technol.*, 306 (2017) 17–25.
- [50] L. Bandura, R. Panek, M. Rotko, W. Franus, Synthetic zeolites from fly ash for an effective trapping of BTX in gas stream, *Microporous Mesoporous Mater.*, 223 (2016) 1–9.
- [51] C. Zhou, T. Sun, Q. Gao, A. Alshameri, P. Zhu, H. Wang, X. Qiu, Y. Ma, C. Yan, Synthesis and characterization of ordered mesoporous aluminosilicate molecular sieve from natural halloysite, *J. Taiwan Inst. Chem. Eng.*, 45 (2014) 1073–1079.
- [52] A. Mayza, D.M. França, F. Wagner, A. Rodrigues, Study of Cu²⁺, Ni²⁺, Zn²⁺ competitive adsorption on synthetic zeolite: an experimental and theoretical approach, *Desal. Water Treat.*, 227 (2021) 263–277.
- [53] S. Hojati, H. Khademi, Cadmium sorption from aqueous solutions onto Iranian sepiolite: kinetics and isotherms, *J. Cent. South Univ.*, 20 (2013) 3627–3632.
- [54] M. Hamidpour, M. Kalbasi, M. Afyuni, H. Shariatmadari, Kinetic and isothermal studies of cadmium sorption onto bentonite and zeolite, *Int. Agrophys.*, 24 (2010) 253–259.
- [55] I.J.M. Duarte, T.M.I. de O. Lima, A.M. de M. França, H.L. de B. Buarque, R.F. do Nascimento, Adsorption of caffeine using steel wastes, *Environ. Sci. Pollut. Res.*, 29 (2022) 79977–79994.
- [56] Z.A. Abadeh, M. Irannajad, Removal of Ni and Cd ions from aqueous solution using iron dust-zeolite composite: analysis by thermodynamic, kinetic and isotherm studies, *Chem. Res. Chin. Univ.*, 33 (2017) 318–326.
- [57] Y. Zhang, J. Dong, F. Guo, Z. Shao, J. Wu, Zeolite synthesized from coal fly ash produced by a gasification process for Ni²⁺ removal from water, *Minerals*, 8 (2018) 116, doi: 10.3390/min8030116.
- [58] M. Mahdavi, M. Bin Ahmad, Md. J. Haron, Y. Gharayebi, K. Shameli, B. Nadi, Fabrication and characterization of SiO₂/(3-aminopropyl)triethoxysilane-coated magnetite nanoparticles for lead(II) removal from aqueous solution, *J. Inorg. Organomet. Polym. Mater.*, 23 (2013) 599–607.
- [59] S.G. Wang, W.X. Gong, X.W. Liu, Y.W. Yao, B.Y. Gao, Q.Y. Yue, Removal of lead(II) from aqueous solution by adsorption onto manganese oxide-coated carbon nanotubes, *Sep. Purif. Technol.*, 58 (2007) 17–23.
- [60] A. Safinejad, N. Goudarzi, M.A. Chamjangali, G. Bagherian, Effective simultaneous removal of Pb(II) and Cd(II) ions by a new magnetic zeolite prepared from stem sweep, *Mater. Res. Express*, 4 (2017) 116104, doi: 10.1088/2053-1591/aa9738.
- [61] M. Visa, Synthesis and characterization of new zeolite materials obtained from fly ash for heavy metals removal in advanced wastewater treatment, *Powder Technol.*, 294 (2016) 338–347.
- [62] H. Baseri, S. Tizro, Treatment of nickel ions from contaminated water by magnetite based nanocomposite adsorbents: effects of thermodynamic and kinetic parameters and modeling with Langmuir and Freundlich isotherms, *Process Saf. Environ. Prot.*, 109 (2017) 465–477.
- [63] N. Saxena, A. Kumar, A. Mandal, Adsorption analysis of natural anionic surfactant for enhanced oil recovery: the role of mineralogy, salinity, alkalinity and nanoparticles, *J. Pet. Sci. Eng.*, 173 (2019) 1264–1283.
- [64] D.S. Tong, C.W. Wu, M.O. Adebajo, G.C. Jin, W.H. Yu, S.F. Ji, C.H. Zhou, Adsorption of methylene blue from aqueous solution onto porous cellulose-derived carbon/montmorillonite nanocomposites, *Appl. Clay Sci.*, 161 (2018) 256–264.
- [65] M.A. Shavandi, Z. Haddadian, M.H.S. Ismail, N. Abdullah, Z.Z. Abidin, Removal of Fe(III), Mn(II) and Zn(II) from palm oil mill effluent (POME) by natural zeolite, *J. Taiwan Inst. Chem. Eng.*, 43 (2012) 750–759.
- [66] B. Sadeghalvad, H.S. Karimi, H. Hosseinzadegan, A.R. Azadmehr, A comparative study on the removal of lead from industrial wastewater by adsorption onto raw and modified Iranian Bentonite (from Isfahan area), *Desal. Water Treat.*, 52 (2014) 6440–6452.